

REGULATION OF THE SPECTRAL PEAK IN GAMMA-RAY BURSTS

ANDREI M. BELOBORODOV

Physics Department and Columbia Astrophysics Laboratory, Columbia University, 538 West 120th Street, New York, NY 10027, USA
Draft version November 5, 2018

ABSTRACT

Observations indicate that the peak of gamma-ray burst spectrum forms in the opaque region of an ultra-relativistic jet. Recent radiative transfer calculations support this picture and show that the spectral peak is inherited from initially thermal radiation, which is changed by heating into a broad photon distribution with a high-energy tail. We discuss the processes that regulate the observed position of the spectral peak E_{pk} . The opaque jet has three radial zones: (1) Planck zone $r < R_{\text{P}}$ where a blackbody spectrum is enforced; this zone ends where Thomson optical depth decreases to $\tau \approx 10^5$. (2) Wien zone $R_{\text{P}} < r < R_{\text{W}}$ with Kompaneets parameter $y \gg 1$ where radiation has a Bose-Einstein spectrum, and (3) Comptonization zone $r > R_{\text{W}}$ where the radiation spectrum develops the high-energy tail. Besides the initial jet temperature, an important factor regulating E_{pk} is internal dissipation (of bulk motions and magnetic energy) at large distances from the central engine. Dissipation in the Planck zone reduces E_{pk} , and dissipation in the Wien zone increases E_{pk} . In jets with sub-dominant magnetic fields, the predicted E_{pk} varies around 1 MeV up to a maximum value of about 10 MeV. If the jet carries an energetically important magnetic field, E_{pk} can be additionally increased by dissipation of magnetic energy. This increase is hinted by observations, which show E_{pk} up to about 20 MeV. We also consider magnetically dominated jets; then a simple model of magnetic dissipation gives $E_{\text{pk}} \approx 30 \Gamma_{\text{W}} \text{ keV}$ where Γ_{W} is the jet Lorentz factor at the Wien radius R_{W} .

Subject headings: plasmas – radiation mechanisms: non-thermal – radiation mechanisms: thermal – radiative transfer – scattering – gamma-rays: bursts, theory – relativity

1. INTRODUCTION

Observed spectra of gamma-ray bursts (GRBs) peak at energy E_{pk} that varies around 1 MeV (after correcting by $1+z$ for the cosmological redshift, Kaneko et al. 2006; Goldstein et al. 2012). The spectrum shape can be described by a simple Band function (Band et al. 2009) — two power laws that are smoothly connected at E_{pk} . Bursts of higher luminosity are observed to have higher E_{pk} . An approximate correlation $E_{\text{pk}} \approx 0.3 L_{\gamma,52}^{1/2} \text{ MeV}$ was reported (e.g. Wei & Gao 2003; Yonetoku et al. 2004; Ghirlanda et al. 2011), where $L_{\gamma,52}$ is the burst luminosity (isotropic equivalent) in units of $10^{52} \text{ erg s}^{-1}$.

The present paper addresses the origin of the spectral peak and the processes that regulate its position.

1.1. Synchrotron model

A simple phenomenological GRB model posits that we observe synchrotron radiation, in analogy with blazar models. The model assumes that a nonthermal electron population is injected in the jet by some dissipative process. It gives a spectrum with

$$E_{\text{pk}} \approx E_s = 0.4 \Gamma \gamma_{\text{peak}}^2 \hbar \frac{eB}{m_e c}. \quad (1)$$

Here B is the magnetic field measured in the rest frame of the jet (“fluid frame”), γ_{peak} is the Lorentz factor at which the injected electron distribution peaks (also measured in the fluid frame), and Γ is the bulk Lorentz factor of the jet itself. If the injection distribution above γ_{peak} is a power-law $dN_e/d\gamma \propto \gamma^{-p}$ then the synchrotron spectrum has a high-energy power-law tail, $dN_\gamma/dE \propto E^{-p/2-1}$ at $E > E_{\text{pk}}$.

One possibility for the injection of high-energy electrons is associated with internal shocks (Rees & Mészáros 1994). A mildly relativistic electron-ion shock produces an electron distribution with $\gamma_{\text{peak}} = \epsilon_e (m_p/m_e)$, where ϵ_e can be a significant fraction of unity. This gives

$$E_{\text{pk}} \approx 1 r_{12}^{-1} \epsilon_B^{1/2} L_{52}^{1/2} \left(\frac{\epsilon_e}{0.3} \right)^2 \text{ MeV}, \quad (2)$$

where r_{12} is radius in units in 10^{12} cm , L_{52} is the isotropic equivalent of the jet power in units of $10^{52} \text{ erg s}^{-1}$, and ϵ_B is the fraction of jet energy that is carried by the magnetic field. If the shock heating radius happens to be $r \sim 10^{13} \epsilon_B^{1/2} \epsilon_e^2 \text{ cm}$ then E_{pk} would be consistent with observations.

Significant, perhaps dominant, magnetic fields are expected in GRB jets. The field is advected by the conducting plasma from the central engine, and plausible scenarios (e.g. hyper-accretion disks around black holes or proto-neutron stars) invoke strong fields. At radii much larger than the size of the central engine the advected field is transverse to the jet direction. Simulations of shocks in the presence of transverse magnetic field with $\epsilon_B > 10^{-4} - 10^{-3}$ show no particle acceleration to high energies $\gamma \gg \gamma_{\text{peak}}$ (Sironi & Spitkovsky 2011). Thus, synchrotron emission from shocks is not expected to extend far above E_{pk} , which conflicts with observations.

The problem with electron acceleration in internal shocks may be avoided if the synchrotron model is viewed more broadly as a phenomenological model that does not specify the origin of nonthermal electrons. When tested against data, the model encounters the following problems.

(1) Thousands of GRBs have been observed, and most

of them have E_{pk} near 1 MeV (Goldstein et al. 2012). Few bursts have E_{pk} above 10 MeV and no bursts are known with $E_{\text{pk}} > 20$ MeV. The synchrotron model does not explain the clustering of E_{pk} around 1 MeV. The model predicts $E_{\text{pk}} \propto \Gamma \gamma_{\text{peak}}^2 B$ which should give a broad distribution — there is no reason for this combination of B , γ_{peak} , and Γ to be comparable in different bursts, or even within one burst, as GRBs are strongly variable.

(2) High-energy electrons quickly cool to $\gamma < \gamma_{\text{peak}}$ (which makes the process radiatively efficient) and should emit radiation at $E < E_{\text{pk}}$ with photon index $\alpha = -3/2$. A typical low-energy index observed in GRBs is $\alpha = -1$, and many bursts have even harder slopes $\alpha > 0$ (Kaneko et al. 2006). The observed hard slopes are in conflict with the synchrotron model.

(3) The observed spectral peak is sharp. E_{pk} is defined as photon energy at which the burst luminosity peaks, i.e. where EL_E is maximum (L_E is the spectral luminosity), and the spectrum shape around the maximum can be quantified by its width at half maximum, $E_1 < E < E_2$. The observed width $\log(E_1/E_2)$ is typically 1-1.5 decades in photon energy. The synchrotron model predicts a broader peak (see e.g. the predicted spectra in Daigne et al. 2011). To make the spectral peak as sharp as possible, one has to assume an unrealistic electron distribution that has a step-like cutoff at $\gamma < \gamma_{\text{peak}}$ (Baring & Braby 2004; Burgess et al. 2011). It is not reasonable to expect a step-like electron distribution for a few reasons. First, no known acceleration process gives the electron distribution with a low-energy cutoff. Second, a low-energy wing of the distribution must be created by the fast electron cooling. Third, many GRBs are highly variable, and the expected variability in γ_{peak} should smear out the cutoff in the time-averaged emission.

Note also that synchrotron spectra with sharp peaks (that could be fitted by a Band function) are not observed in any other astrophysical objects. A close example is provided by blazar spectra (e.g. Ghisellini 2006). Their synchrotron spectra have the half-maximum width of several orders of magnitude, much broader than in GRBs.

The problems of the synchrotron model are shared by other versions of optically thin emission, e.g. jitter radiation. Observations suggest that the GRB spectral peak forms in the opaque region of the jet.

1.2. Photospheric emission

In the opaque jet, photons keep interacting with the plasma and their spectrum is expected to take a well defined shape with a sharp peak. (For example, consider the extreme case of a Planck distribution.) The radiation is released near the photospheric radius R_* , and a distant observer will see a spectrum with a sharp peak.

The simplest model of photospheric emission assumes a freely expanding radiation-dominated outflow with no baryon loading or magnetic field (Paczynski 1986; Goodman 1986). It was recently shown that the emission received by distant observers from such outflows has a Planck spectrum (Beloborodov 2011). The peak energy of the Planck spectrum is related to the average photon energy \bar{E} by $E_{\text{pk}} \approx 1.45\bar{E}$. In the ideal radiation-dominated outflow \bar{E} remains constant, equal to its value

near the central engine E_0 .

In general, E_0 may be expressed in terms of the jet power L_0 and the initial radius r_0 (comparable to the size of the central compact object),

$$E_0 \approx 10 \epsilon_0^{1/4} L_{0,52}^{1/4} r_{0,6}^{-1/2} \text{ MeV}, \quad (3)$$

where ϵ_0 is the initial thermal fraction of the power L_0 . Radiation-dominated jets have $\epsilon_0 = 1$. Their predicted $E_{\text{pk}} \approx 1.45E_0$ may be made consistent with observed $E_{\text{pk}} \sim 0.3 L_{\gamma,52}^{1/2}$ MeV if r_0 is large and the flow is collimated within a small angle θ_b , which reduces the true jet power, $L_0 \approx (\theta_b^2/2)L_\gamma$.

This simple model, however, fails to explain the observed spectra. Although the Planck spectrum may appear in the time-resolved emission of some bursts (e.g. Ryde et al. 2011), GRB spectra are typically nonthermal, with an extended high-energy tail.

Theoretically, GRB jets may be expected to carry baryons and magnetic fields, and this more detailed model offers an explanation of the observed spectra. Two types of jets may be considered:

(1) *Thermally dominated baryon-loaded jets*: at small radii the jet is dominated by the thermal energy of radiation (and e^\pm pairs). The expanding fluid cools adiabatically and its thermal energy is converted to the bulk kinetic energy of the baryonic flow (Paczynski 1990; Shemi & Piran 1990). Any subphotospheric heating is expected to change the spectrum emitted at the photosphere (e.g. Eichler & Levinson 2000; Rees & Mészáros 2005; Pe'er et al. 2006). In particular, collisional dissipation was shown to peak at Thomson optical depths $\tau \sim 10$ and its detailed calculations yielded spectra consistent with observations (Beloborodov 2010; Vurm et al. 2011). The calculations show that synchrotron emission significantly contributes to the photospheric emission at $E < E_{\text{pk}}$ but never dominates the spectral peak. The peak is dominated by radiation that has been thermalized at radii $r \ll R_*$.

(2) *Magnetically dominated jets*: at small radii the jet energy in the fluid frame is dominated by the magnetic field. In the lab frame, the jet luminosity is dominated by the Poynting flux. The magnetic field gradually dissipates and the jet Lorentz factor grows with radius. For instance, Drenkhahn & Spruit (2002) considered an alternating magnetic field that dissipates via reconnection. The jet also carries baryons, and the ultimate result of dissipation can be the conversion of magnetic energy to the bulk kinetic energy of baryons, with some radiative losses. This gradual conversion can take several decades in radius; it peaks at a radius R_{diss} which may or may not be comparable to the photospheric radius R_* . Another uncertainty is the unknown effect of magnetic dissipation on the electron distribution. Assuming Maxwellian electrons, Giannios (2008) calculated the radiation produced by magnetic dissipation. The predicted spectra are in reasonable agreement with observed GRBs if R_{diss} is comparable to R_* .

Radiative transfer in a heated subphotospheric region has been studied with four different numerical codes (Pe'er et al. 2006; Giannios 2008; Beloborodov 2010; Vurm et al. 2011), consistently giving Band-type spectra. These calculations show how the spectrum broadens from the thermal to Band shape at optical depths

$\tau \lesssim 30$. The resulting E_{pk} at $\tau \sim 1$ is weakly changed from its value at $\tau \sim 30$ (Beloborodov 2010; Giannios 2012).¹ Thus, E_{pk} is mainly regulated at smaller radii where $\tau \gg 30$. We focus in this paper on radiative processes that occur in this highly opaque zone.

1.3. Photon production and E_{pk}

The processes regulating the peak of the photospheric spectrum are more sophisticated than assumed in existing data analysis. The simplest estimate $E_{\text{pk}} \approx 4\Gamma kT_{\text{eff}}$ associates E_{pk} with the effective temperature of the photosphere T_{eff} , which is defined by

$$\frac{4}{3} aT_{\text{eff}}^4 \Gamma^2 4\pi R_{\star}^2 c = L_{\gamma}. \quad (4)$$

The estimate $E_{\text{pk}} \approx 4\Gamma kT_{\text{eff}}$ simply posits a blackbody photospheric emission. In fact, it should be viewed as a lower limit for E_{pk} , not its true value.

An improved estimate assumes that radiation is blackbody at $r \sim R_{\text{W}}$ instead of $r \sim R_{\star}$ (Giannios 2012). This assumption can still significantly underestimate E_{pk} . The more realistic model should not make blackbody assumptions at any radii. Instead, it must address the number of photons produced in the jet. This number is typically not sufficient to maintain a blackbody spectrum with $T = T_{\text{eff}}$. The same luminosity L_{γ} carried by a smaller number of photons implies a higher E_{pk} .

The radiative processes that control the photon number in the opaque thermal plasma are detailed in Section 2. The problem resembles the evolution of radiation in the early universe, although the early universe is known to be much less dissipative than GRB jets — the observed cosmic microwave background has a nearly Planck spectrum and provides stringent upper limits on subphotospheric dissipation. Section 2 also briefly discusses the (uncertain) role of nonthermal processes at high optical depths. Sections 3 and 4 consider thermally and magnetically dominated jets, respectively. The results are discussed in Section 5.

2. PLANCK AND WIEN ZONES

2.1. Notation

We first introduce notation for basic quantities that will be used in this paper. Let $dL/d\Omega$ be the jet power per unit solid angle; the corresponding isotropic equivalent is defined by $L = 4\pi (dL/d\Omega)$. The power is carried by photons, baryons, electrons, e^{\pm} pairs, and magnetic field. The baryonic component includes protons and neutrons; the neutron-to-proton ratio depends on the details of the central engine (Beloborodov 2003). An important parameter of the jet is its energy per proton,

$$\eta = \frac{L}{\dot{M}c^2}, \quad (5)$$

where $\dot{M} = 4\pi (d\dot{M}/d\Omega)$ is the proton mass outflow rate (isotropic equivalent). The proton number density in the

¹ Radiative transfer calculations show that, without subphotospheric heating, adiabatic cooling would reduce E_{pk} by a factor of $2\tau^{-2/3}$ (Beloborodov 2011). Heating offsets this effect. In the Comptonization zone $\tau < 10^2$, the subphotospheric heating is also spent to create the high-energy tail of the spectrum, which limits the growth of E_{pk} . As a result, E_{pk} remains roughly constant in the Comptonization zone.

rest frame of the jet (“fluid frame”) is given by

$$n = \frac{\dot{M}}{4\pi r^2 m_p c \Gamma}, \quad (6)$$

where $\Gamma(r)$ is the Lorentz factor of the jet. In addition to the proton-electron plasma the jet may contain e^{\pm} pairs of density n_{\pm} .

The expansion timescale measured in the fluid frame is given by

$$t_{\text{exp}} = \frac{r}{c\Gamma}, \quad (7)$$

and the characteristic optical depth of the jet at a radius r is

$$\tau = \frac{(n + n_{\pm}) \sigma_{\text{T}} r}{\Gamma}. \quad (8)$$

We will focus on the opaque region $\tau \gg 1$.

The radiation component of the jet power (isotropic equivalent) can be expressed as

$$L_{\gamma} = 4\pi r^2 \frac{4}{3} U_{\gamma} \Gamma^2 c, \quad (9)$$

where U_{γ} is the radiation energy density in the fluid frame, and $(4/3)U_{\gamma}$ is the radiation enthalpy. The fraction of the total jet power that is carried by radiation is

$$\epsilon = \frac{L_{\gamma}}{L} = \frac{4}{3} \frac{\Gamma U_{\gamma}}{\eta n m_p c^2}. \quad (10)$$

As the jet expands, ϵ may evolve as a result of adiabatic cooling and dissipative heating.

The magnetic (Poynting flux) component of the jet power is

$$L_B = r^2 B^2 \Gamma^2 c. \quad (11)$$

In this paper, the magnetic fraction will be defined by

$$\epsilon_B = \frac{L_B}{L}, \quad (12)$$

i.e. normalized to the total jet power, so that $\epsilon_B \leq 1$.

2.2. Planck zone

The central engines of GRBs are hot and fill their jets with blackbody radiation of a high temperature. As the jet expands, the Planck spectrum is initially enforced by huge rates of photon emission and absorption. The number density of Planck photons at temperature T is given by

$$n_{\text{P}} \approx \frac{0.2}{\lambda^3} \Theta^3, \quad \Theta = \frac{kT}{m_e c^2}, \quad (13)$$

where $\lambda = \hbar/m_e c$ is Compton wavelength. The temperature of blackbody radiation is determined by its energy density, $aT^4 = U_{\gamma}$, where $a = \pi^2 k^4 / 15c^2 \hbar^3$.

There is a characteristic “Planck radius” R_{P} inside of which radiative processes in the thermal plasma are fast enough to enforce a Planck spectrum. Outside R_{P} photon production becomes inefficient and the photon number freezes out (until the jet expands to radii where nonthermal processes may produce significant synchrotron radiation). Below we show that the jet temperature at R_{P} is $\Theta_{\text{P}} \approx 0.01 - 0.02$, almost independent of the GRB parameters.

Two radiative processes should be considered in the thermal plasma: bremsstrahlung $e + p \rightarrow e + p + \gamma$ and double Compton effect $e + \gamma \rightarrow e + \gamma + \gamma$. Let \dot{n}_B and \dot{n}_{DC} be the rates of photon production by these two processes [$\text{cm}^{-3} \text{s}^{-1}$]. In a plasma with approximately Planckian radiation the rates are given by

$$\dot{n}_B = \xi n^2 \sigma_{Tc} \Theta^{-1/2}, \quad (14)$$

$$\dot{n}_{DC} = \chi n_\gamma n \sigma_{Tc} \Theta^2, \quad (15)$$

where the numerical factors $\xi \approx 0.06$ and $\chi \approx 0.1$ weakly (logarithmically) depend on Θ (see Appendix). When evaluating the rates of photon production we neglected the presence of e^\pm pairs; this approximation is reasonable as will be discussed below. The total rate of photon production is $\dot{n}_\gamma = \dot{n}_{DC} + \dot{n}_B$.

Ratio $\dot{n}_{DC}/\dot{n}_B \approx 2(n_\gamma/n)\Theta^{5/2}$ is sensitive to temperature and also depends on the photon-to-baryon ratio, which may be evaluated as

$$\frac{n_\gamma}{n} = \frac{L_\gamma m_p}{\bar{E} M} = \frac{\epsilon \eta m_p c^2}{\bar{E}} = 3 \times 10^5 \epsilon \left(\frac{\eta}{300} \right) \left(\frac{\bar{E}}{\text{MeV}} \right)^{-1}. \quad (16)$$

Using $n_\gamma/n \sim 10^5$, one concludes that $\dot{n}_{DC} > \dot{n}_B$ for $\Theta \gtrsim 0.01$.² For the estimates of the boundary of the Planck zone we will use the approximation $\dot{n}_\gamma \approx \dot{n}_{DC}$.

The balance between emission and absorption of Planck photons is maintained as long as $\dot{n}_\gamma t_{\text{exp}} > n_\gamma$, and radius R_P is defined by the following condition,

$$t_{\text{exp}} \dot{n}_{DC} = n_\gamma. \quad (17)$$

Substituting Equations (7) and (15), and using Equation (8) with $n_\pm \ll n$, we can rewrite the condition (17) as

$$\Theta^2 \tau = \chi^{-1}. \quad (18)$$

As radiation is still approximately blackbody at $r \sim R_P$, we can use $aT^4 \approx U_\gamma$ and substitute U_γ from Equation (10). This gives,

$$T \approx T_{\text{eff}} = \left(\frac{3\epsilon\eta n m_p c^2}{4\Gamma a} \right)^{1/4} = \left(\frac{3\epsilon\eta m_p c^2 \tau}{4a\sigma_{Tc}} \right)^{1/4}. \quad (19)$$

From Equations (18) and (19), we find Θ at the Planck radius,

$$\begin{aligned} \Theta_P &= \left(\frac{45}{4\pi^2 \chi} \frac{m_p}{m_e} \epsilon_P \eta \frac{\lambda^3}{\sigma_{Tc} R_P} \right)^{1/6} \\ &\approx 1.1 \times 10^{-2} R_{P,10}^{-1/6} \epsilon_P^{1/6} \eta_2^{1/6}. \end{aligned} \quad (20)$$

The scattering optical depth at the Planck radius is

$$\tau_P = (\chi \Theta_P^2)^{-1} \sim 10^5. \quad (21)$$

Note that Θ_P and τ_P weakly depend on the exact value of R_P , which can be determined in concrete jet models discussed in Sections 3 and 4.

Our calculation of Θ_P neglected e^\pm pairs. This approximation is easy to check for the thermal plasma. At $r \lesssim R_P$ pair annihilation balance is maintained with

² This conclusion may not hold if the jet is polluted with clumps or sheets with a low entropy per baryon. In such clumps bremsstrahlung could dominate photon production.

approximately blackbody radiation field. At $\Theta \ll 1$ it gives the following equation for positron density n_+ (e.g. Svensson 1984),

$$\frac{n_+^2}{n_+(n_+ + n)} = \frac{8\zeta(3)}{\pi} \Theta^3 \exp\left(\frac{2}{\Theta}\right), \quad (22)$$

where $\zeta(3) \approx 1.2$ is the Riemann zeta function. One can see that $n_+ \ll n$ at $\Theta = \Theta_P$.

2.3. Wien zone

Compton scattering maintains a Bose-Einstein distribution of photons as long as Kompaneets parameter

$$y = 4\Theta\tau \gg 1. \quad (23)$$

Comptonization with $y \gg 1$ enforces a common electron-photon temperature, $T_e = T_\gamma = T$. The strong thermal coupling between photons and electrons may also be viewed from the electron point of view. The condition $y \gg 1$ is equivalent to $(3/2)nkT/t_C \gg U_\gamma/t_{\text{exp}}$ where $t_C = 3m_e c/8\sigma_{Tc} U_\gamma$ is the timescale for electron temperature relaxation to the radiation temperature.

The Bose-Einstein distribution is described by the photon occupation number

$$\mathcal{N} = \frac{1}{\exp(\mu + x) - 1}, \quad x = \frac{h\nu}{kT}, \quad (24)$$

where chemical potential $\mu \geq 0$ describes the deficit of photon density compared with the Planck value n_P . In the Planck zone, the distribution takes the Planck form ($\mu \ll 1$) with $n_\gamma = n_P$. Outside the Planck radius the photon number freezes out and, in a heated jet, $n_\gamma/n_P < 1$. Thermalized radiation with $n_\gamma \ll n_P$ is described by $\mu \gg 1$; then radiation has a Wien spectrum $\mathcal{N} \approx \exp(-\mu - x)$.

Hereafter we call the region where $y > 1$ the ‘‘Wien zone’’ to emphasize the possibility of $\mu \gg 1$ outside R_P . More exactly, photons must have a Bose-Einstein distribution where $y \gg 1$; whether $\mu \gg 1$ is satisfied depends on the heating history. The average photon energy in the fluid frame is between $2.7kT$ (Planck) and $3kT$ (Wien). Radiation energy density in the Wien zone is given by

$$U_\gamma \approx 3kT n_\gamma, \quad r < R_W. \quad (25)$$

As the photon density n_γ may be below $n_P = aT^4/2.7kT$, the radiation density U_γ may be below the blackbody value aT^4 .

Equations (10) and (25) give the following expression for the photon-to-baryon ratio,

$$\frac{n_\gamma}{n} = \frac{\eta m_p}{4m_e} \frac{\epsilon}{\Gamma \Theta}. \quad (26)$$

The average photon energy in the fixed lab frame (also the frame of a distant observer) is given by

$$\bar{E} = \frac{\epsilon \eta m_p c^2}{n_\gamma/n} = 4\Gamma kT. \quad (27)$$

The thermal (Bose-Einstein) spectrum peaks at a photon energy that is slightly above \bar{E} ,

$$E_{\text{pk}} = \bar{E} \times \begin{cases} 1.45 & \text{Planck} \\ \frac{4}{3} & \text{Wien} \end{cases} \quad (28)$$

The observed photospheric spectrum is changed from the Wien shape by Comptonization outside the Wien zone; however, E_{pk} weakly evolves outside R_{W} . Thus, the observed E_{pk} may be estimated as \bar{E}_{W} , which is given by

$$\bar{E}_{\text{W}} \approx \frac{\epsilon_{\text{W}}}{\epsilon_{\text{P}}} \bar{E}_{\text{P}} \approx \frac{\epsilon_{\text{W}}}{\epsilon_{\text{P}}} 4\Gamma_{\text{P}} kT_{\text{P}}. \quad (29)$$

Here index ‘‘P’’ indicates that the quantity is evaluated at the Planck radius and index ‘‘W’’ — at the Wien radius. Equation (29) assumes that the photon number carried by the jet is not significantly changed outside the Planck zone; then $\bar{E} \propto \epsilon$ between R_{P} and R_{W} . Section 2.2 showed that $kT_{\text{P}} = 5 - 10$ keV, as long as photon production is dominated by the thermal plasma. Then,

$$E_{\text{pk}} \approx 30\Gamma_{\text{P}} \frac{\epsilon_{\text{W}}}{\epsilon_{\text{P}}} \text{ keV}. \quad (30)$$

The optical depth at the Wien radius R_{W} may be expressed in terms of Θ_{W} from $y \approx 1$,

$$\tau_{\text{W}} \approx \frac{1}{4\Theta_{\text{W}}} \approx \frac{\Gamma_{\text{W}} m_e c^2}{E_{\text{pk}}}. \quad (31)$$

Maintaining the Bose-Einstein spectrum requires $y \gg 1$, which corresponds to $\tau \gg \tau_{\text{W}}$.

2.4. Evolution equation for photon-to-baryon ratio

The transition between the Planck and Wien zones is more accurately described by an evolution equation for n_{γ}/n . Using $dt = dr/\Gamma c$ (where t is the proper time measured in the fluid frame) the rate of change of n_{γ}/n may be written as

$$\frac{d}{dr} \left(\frac{n_{\gamma}}{n} \right) = \frac{\dot{n}_{\gamma}}{n\Gamma c}, \quad (32)$$

where \dot{n}_{γ} is the net rate of photon production measured in the fluid frame,

$$\dot{n}_{\gamma} = (\dot{n}_{\text{B}} + \dot{n}_{\text{DC}}) \left(1 - \frac{n_{\gamma}}{n_{\text{P}}} \right). \quad (33)$$

Here $n_{\text{P}}(\Theta)$ is the Planck density (Equation 13), and the factor $(1 - n_{\gamma}/n_{\text{P}})$ takes into account photon absorption; the net photon production rate vanishes when $n_{\gamma} = n_{\text{P}}$ as expected from detailed balance for blackbody radiation.

To obtain the equation for function $f(r) = n_{\gamma}/n$ first note that temperature is related to f by Equation (26), which we rewrite as

$$\Theta = \frac{H}{f}, \quad H(r) = \frac{\eta m_{\text{p}}}{4m_e} \frac{\epsilon(r)}{\Gamma(r)}. \quad (34)$$

Then from Equation (32) we obtain,

$$\frac{df}{d \ln r} = \tau \left(\xi \frac{f^{1/2}}{H^{1/2}} + \chi \frac{H^2}{f} \right) \left(1 - \frac{\lambda^3 n f^4}{0.2 H^3} \right). \quad (35)$$

This equation is easily solved for $f(r)$ for any concrete jet model with given $\Gamma(r)$, $n(r)$, and heating history $\epsilon(r)$. The solution also determines $\Theta(r) = H/f$.

2.5. Nonthermal processes

We focus in this paper on the early, opaque stages of expansion and consider thermal heating of the jet due

to dissipation of internal bulk motions or magnetic energy. It is, however, possible that dissipation also generates high-energy nonthermal particles, even at very high optical depths. This possibility is questionable for internal shocks — it was argued that shocks at high optical depths are mediated by radiation and have a considerable thickness, comparable to the photon free path (Levinson 2012); such shocks would be unable to accelerate electrons. Nonthermal electrons can be generated by magnetic reconnection, although the efficiency of this process is uncertain. High-energy electrons produce synchrotron photons that can be Comptonized to the Wien peak and contribute to n_{γ} (Thompson et al. 2007).

Here we limit our discussion to the following estimate. Suppose a fraction ϵ_{nth} of the jet power L is given to accelerated electrons. They immediately radiate this power via inverse Compton scattering and synchrotron losses. Scattering does not change photon number, so only the synchrotron luminosity is relevant, which is given by

$$L_s = \frac{U_B}{f_{\text{KN}} U_{\gamma} + U_B} \epsilon_{\text{nth}} L = \frac{\epsilon_B/2}{f_{\text{KN}}(3/4)\epsilon + \epsilon_B/2} \epsilon_{\text{nth}} L. \quad (36)$$

Here $U_B = B^2/8\pi$, ϵ_B and ϵ are the fractions of jet energy carried by the magnetic field and radiation, respectively; the factor $f_{\text{KN}} < 1$ describes the Klein-Nishina correction to Compton losses.

The synchrotron power L_s peaks at energy E_s given by Equation (1), assuming γ_{peak} is high enough to avoid synchrotron self-absorption. The produced photon number, however, peaks at the low end of the synchrotron spectrum. The photon production may be roughly estimated as³

$$\dot{N}_s \approx \frac{L_s}{E_s} \left(\frac{E_s}{E_{\text{abs}}} \right)^{1/2}, \quad (37)$$

where E_{abs} is the energy above which soft photons are Comptonized to the Wien peak faster than absorbed. Photons may be self-absorbed by the high-energy electrons or absorbed by the thermal plasma via inverse double Compton effect (Appendix); typically $E_{\text{abs}} \sim 10^{-2} \bar{E}$. More careful calculations take into account the induced downscattering (Bose condensation) of the synchrotron photons on the thermal electrons, which increases the effective E_{abs} (Vurm et al. 2012).

Comparing \dot{N}_s with the existing flux of thermal photons, one finds

$$\frac{\dot{N}_s}{\dot{N}_{\gamma}} \approx \frac{\epsilon_{\text{nth}} \epsilon_B}{\epsilon \left(\frac{3}{2} f_{\text{KN}} \epsilon + \epsilon_B \right)} \frac{\bar{E}}{E_s} \left(\frac{E_s}{E_{\text{abs}}} \right)^{1/2}. \quad (38)$$

Synchrotron emission does not appreciably change the photon number carried by the jet when this ratio is smaller than unity. The highest \dot{N}_s is achieved if $E_s \sim E_{\text{abs}}$. Even this maximum rate may be insufficient to significantly influence the photon number at large optical depths; it depends on the unknown ϵ_{nth} and the Lorentz factors of the accelerated particles.

³ The power index of $(E_s/E_{\text{abs}})^{1/2}$ in this equation comes from the standard synchrotron spectrum of fast-cooling electrons; it may be slightly changed if the injected electron distribution is modified by e^{\pm} cascade accompanying inverse Compton scattering.

3. THERMALLY DOMINATED JETS

3.1. Non-dissipative jet

Early works on GRBs studied in detail the dynamics of ideal (non-dissipative) relativistic hot outflows loaded with baryons (e.g. Paczyński 1990; Shemi & Piran 1990). The flow acceleration is controlled by parameter η (Equation 5). In a radial flow, the fluid Lorentz factor Γ grows linearly with r until it approaches its maximum value $\Gamma = \eta$ at $R_s \sim \eta r_0$.

The photospheric radius R_\star is defined by $\tau = 1$; it is given by

$$R_\star = \frac{L\sigma_T(1 + n_\pm/n)}{4\pi m_p c^3 \Gamma^2 \eta}. \quad (39)$$

We will consider here jets with $R_\star > R_s$, so that $\Gamma \approx \eta$ at the photosphere. In the absence of dissipation, the density of relict e^\pm pairs is negligible at R_\star , $n_\pm/n \ll 1$.

In the non-dissipative jet, the evolution of radiation is fully controlled by adiabatic cooling. Entropy is dominated by radiation and proportional to the photon number; thus, adiabatic cooling conserves photon number. The photon-to-baryon ratio n_γ/n remains constant as the jet expands;⁴ it is set by the initial conditions at radius r_0 ,

$$\frac{n_\gamma}{n} \approx 240 \eta r_{0,7}^{1/2} L_{0,52}^{-1/4}. \quad (40)$$

At radii $r < R_s$, where the jet power is dominated by radiation, $L_\gamma \approx L$, the constancy of the total fluxes of energy and photon number implies a constant energy per photon $\bar{E}(r) = L_\gamma/\dot{N}_\gamma = \text{const}$. Adiabatic cooling of photons in the fluid frame is compensated by the increasing Doppler shift as the jet accelerates, $\bar{E} \propto T\Gamma = \text{const}$.

At radii $R_s < r < R_\star$, radiation continues to cool adiabatically, $T \propto n^{1/3} \propto r^{-2/3}$ while $\Gamma \approx \text{const} = \eta$. Its spectrum is still blackbody, the photon number is still conserved, and L_γ is decreasing, $L_\gamma \propto T \propto r^{-2/3}$. As a result, \bar{E} and L_γ are reduced between R_s and R_\star by a factor of $\sim (R_\star/R_s)^{-2/3}$. This gives

$$\bar{E}(R_\star) \approx 4\eta^{8/3} L_{52}^{-5/12} r_{0,7}^{1/6} \text{ MeV}. \quad (41)$$

This standard estimate (e.g. Paczynski 1990) is refined by a factor of two by accurate radiative transfer calculations (Beloborodov 2011). The predicted photospheric emission $L_\star \approx (\bar{E}_\star/E_0)L$ is bright and has a high $E_{\text{pk}} > 1$ MeV if the jet has $\eta \gtrsim 600L_{52}^{5/32}$. Its spectrum cuts off exponentially above $\bar{E}(R_\star)$.

3.2. Dissipative jet

Dissipation can offset adiabatic cooling between R_s and R_\star and keep L_γ close to the total jet power L . Heating is especially important for bursts with $R_\star \gg R_s$ where adiabatic cooling threatens to greatly reduce E_{pk} .

Deep subphotospheric heating is expected, in particular if $R_\star \gg R_s$, because such jets have moderate Lorentz factors Γ and thus internal dissipation should start early.

⁴ More exactly, the photon-to-baryon ratio is $n_\gamma/(n+n_n)$ where n_n is the number density of neutrons. For simplicity, we assume a constant proton fraction $Y_c = n/(n+n_n)$ and use n_γ/n as a conserved ‘‘photon-to-baryon ratio.’’

For instance, internal shocks can form and propagate at all radii $r > \Gamma^2\lambda$, where λ is the minimum scale of the Lorentz factor variations, possibly comparable to the size of the central compact object $\sim 10^6$ cm. The energy density in the shock is dominated by radiation and protons. In the region of large optical depth $\tau \gg 10$ the proton heat is quickly shared with electrons via Coulomb collisions (Beloborodov 2010), and Compton scattering immediately passes the heat to radiation, which dominates the heat capacity of the jet by a huge factor $\sim n_\gamma/n$.

Similar electron/photon heating is expected in the presence of any mechanism that stirs protons and gives them random motions in the fluid frame. It may result from magnetic reconnection. Dissipation of subdominant magnetic field $B^2/8\pi \lesssim nm_p c^2$ is sufficient to give thermal energy $\lesssim E_0$ per photon and keep \bar{E} from falling far below E_0 .

Coulomb electron heating continues at $r > R_W$ where it leads to $T_e > T_\gamma$ and Comptonization of Wien radiation into a Band spectrum. Coulomb heating is a two-body process and its efficiency decreases proportionally to optical depth τ as the jet approaches the photosphere. The resulting photospheric spectrum is shaped by heating and transfer effects at optical depths $\tau \sim 10$.

Besides the thermal Coulomb heating, the spectrum is affected by electrons that are injected with energies $\gamma m_e c^2 \sim m_\pi c^2 \approx 140$ MeV by n - p or p - p collisions. These electrons produce additional high-energy photons via inverse Compton scattering and low-energy photons via synchrotron emission. Detailed calculations of these processes and their effects on the photospheric spectrum are found in Beloborodov (2010) and Vurm et al. (2011).

The peak energy of the emerging spectrum is inherited from the thermal plasma at large optical depths $\sim \tau_W \sim 10^2$.⁵ It depends on the photon-to-baryon ratio n_γ/n , which can freeze out at the Planck radius R_P as discussed in Section 2. A high radiative efficiency $\epsilon \sim 1$ is expected in the dissipative jet, and then Equation (30) gives

$$E_{\text{pk}} \approx 30 \Gamma_P \text{ keV}. \quad (42)$$

i.e. E_{pk} is determined by the jet Lorentz factor at the Planck radius. A typical GRB with $E_{\text{pk}} \sim 1$ MeV has $\Gamma_P \sim 30$; the highest observed E_{pk} corresponds to $\Gamma_P \sim 300$. Note that the photon freeze-out can occur before the jet acceleration is complete, as Γ_P can be smaller than the final Lorentz factor $\Gamma \approx \eta$.

The maximum possible E_{pk} corresponds to radiative efficiency $\epsilon = 1$ and the minimum photon number n_γ/n . Since dissipation can only increase n_γ/n from its central value $(n_\gamma/n)_0$, the maximum E_{pk} is achieved if $n_\gamma/n = (n_\gamma/n)_0$. It corresponds to

$$\bar{E}_W^{\text{max}} = E_0, \quad (43)$$

where E_0 is given by Equation (3). The maximum $E_{\text{pk}} \sim E_0$ is achieved if the flow is adiabatic in the Planck zone and dissipative in the Wien zone (maintaining $\epsilon \sim 1$).

⁵ E_{pk} is close to but slightly different from \bar{E} , depending on the spectrum shape. In particular, $E_{\text{pk}} \approx 1.45\bar{E}$ for a Planck spectrum and $E_{\text{pk}} = (4/3)\bar{E}$ for a Wien spectrum. The main effect of Comptonization at $r > R_W$ is to create a high-energy tail above E_{pk} , and it also slightly affects E_{pk} itself. Here we neglect the shift of E_{pk} between R_W and R_\star .

Then the expansion at $r < R_P$ gives $\Gamma_P \approx T_0/T_P \approx E_0/3kT_P$.

If the Planck zone is not adiabatic (i.e. the flow is dissipative), the photon number is increased by a factor $Q > 1$. At the same time, Γ_P is reduced by the factor Q^{-1} (so that the jet carries the same luminosity $L_\gamma \approx L$ and the energy conservation law is satisfied). Then E_{pk} is also reduced by Q^{-1} ,

$$\frac{n_\gamma}{n} = Q \left(\frac{n_\gamma}{n} \right)_0, \quad \Gamma_P = \frac{\Theta_0}{Q\Theta_P}, \quad E_{\text{pk}} \approx \epsilon \frac{E_0}{Q}. \quad (44)$$

The Planck radius may be evaluated using Equation (18) and the expression for the optical depth,

$$\tau_P = \frac{L\sigma_T}{4\pi R_P m_p c^3 \eta \Gamma_P^2} = \frac{1}{\chi \Theta_P^2}. \quad (45)$$

As long as the main producer of photons in the GRB spectral peak is the opaque thermal plasma, we can use $\Gamma_P \approx (\epsilon_P/\epsilon)(E_{\text{pk}}/4kT_P\epsilon)$, where E_{pk} is the observed peak position. Then Equation (45) gives,

$$R_P \approx \frac{4\chi\sigma_T L}{\pi m_p c^3 \eta} \left(\frac{\epsilon_P}{\epsilon} \frac{E_{\text{pk}}}{m_e c^2} \right)^{-2} \Theta_P^4. \quad (46)$$

Combining with Equation (20) for Θ_P , we find

$$R_P \approx 10^{10} \epsilon^{3/5} \epsilon_P^{-4/5} \eta_2^{-1/5} L_{\gamma,52}^{3/5} \left(\frac{E_{\text{pk}}}{300 \text{ keV}} \right)^{-6/5} \text{ cm}. \quad (47)$$

The observed bursts typically have $E_{\text{pk}} \sim 300 L_{\gamma,52}^{1/2}$ keV (although some bursts deviate from this relation, e.g. bursts with the highest E_{pk}); this is consistent with approximately constant $R_P \sim 10^{10}$ cm.

3.3. Collimation

Achromatic breaks in GRB afterglow light curves are often interpreted as evidence for jet beaming, with a typical opening angle of 5-10°. Beaming helps explain the extremely high apparent luminosities, up to 10^{54} erg s⁻¹ in some GRBs. Beaming must be achieved through a collimation process. It is expected from the pressure confinement of the jet by the progenitor star or by a non-relativistic dense wind from the outer regions of the accretion disk around the central object. What effect can collimation have on observed E_{pk} ?

If collimation is not accompanied by significant dissipation, the expanding jet can be described as an ideal relativistic flow confined by a wall that determines the cross section of the jet $S(r) = S_0(r/r_0)^\psi$, where r is the radial distance along the jet axis and r_0 is the size of the central engine. For instance, a parabolic wall gives $S(r) \propto r$, i.e. $\psi = 1$, and uncollimated (radial) expansion is described by $\psi = 2$. The opening angle of the jet is determined by ψ and the radius R_{coll} where the wall ends and free expansion begins (e.g. where the jet escapes the progenitor star). Between r_0 and R_{coll} the opening angle decreases as $\theta_b \approx (r_0/r)^{1-\psi/2}$. The jet Lorentz factor in the collimation funnel grows as $\Gamma \approx (r/r_0)^{\psi/2}$ while its temperature decreases as Γ^{-1} (as required by conservation laws, see e.g. Section 3.1 in Beloborodov 2003). Note that in the funnel $\Gamma\theta_b \approx 1$; it implies a marginal

causal contact across the jet. A typical beaming angle $\theta_b \sim 0.1$ at R_{coll} corresponds to $\Gamma \sim 10 \ll \eta$ and temperature $\Theta \sim 0.1\Theta_0 > \Theta_P$, i.e. collimation is expected to occur in the Planck zone $r < R_P$.

Dissipationless collimation conserves entropy, and hence does not change photon-to-baryon ratio n_γ/n . This implies conservation of the total photon number carried by the jet. It also implies that collimation does not change the average photon energy, \bar{E} . Beaming boosts the isotropic equivalent of luminosity $L_\gamma \approx L$ and the isotropic equivalent of photon flux \dot{N}_γ by the same factor $\sim \theta_b^{-2} = (R_{\text{coll}}/r_0)^{2-\psi}$. Their ratio $\bar{E} = L_\gamma/\dot{N}_\gamma$ remains unchanged from its value at r_0 , $\bar{E} = E_0$. Then photospheric emission has $\bar{E} = \epsilon E_0$ as discussed Section 3, so a radiatively efficient burst with $\epsilon \sim 1$ basically inherits \bar{E} (and hence E_{pk}) from the central region $r \sim r_0$ even though L may be strongly increased by beaming.

Next consider dissipative collimation, for instance collimation accompanied by shocks (e.g. Lazzati et al. 2009). Dissipation generates entropy and hence increases n_γ/n . Thus, the total photon number carried by the jet is increased, $Q > 1$, and hence \bar{E} (jet energy per photon) is reduced.

If there is a relation between θ_b and Q , it leads to a correlated variation of L and E_{pk} (with θ_b being the varying parameter). Note that θ_b must satisfy $\Gamma\theta_b \lesssim 1$ for a causal contact across the jet. This condition is marginally satisfied for ideal (non-dissipative) collimation and easily satisfied for dissipative collimation, as it reduces Γ while increasing the jet internal energy.

Thompson et al. (2007) considered the possibility that θ_b always tends to its maximum allowed value $\theta_b \sim \Gamma^{-1}$. They pointed out that this gives $\bar{E} \propto \theta_b^{-1}$ and hence $E_{\text{pk}} \propto L^{1/2}$, similar to the observed trend. Their model encounters, however, two difficulties. First, it has to invoke large variations in θ_b , not only from burst to burst but also within a single burst (as an extended $E_{\text{pk}}-L_\gamma$ correlation was reported in individual GRBs, e.g. Ghirlanda et al. 2011). Second, the model posits that GRBs of various apparent luminosities $L \sim L_0\theta_b^{-2}$ have approximately the same true power $L_0 \sim 10^{50}$ erg s⁻¹, which implies a central temperature $kT_0 \approx 1r_{0,6}^{-1/2}$ MeV. Then the brightest bursts have the highest $E_{\text{pk}} \approx 3kT_0 \approx 3r_{0,6}^{-1/2}$ MeV. It falls short of the observed highest $E_{\text{pk}} \sim 15$ MeV.

3.4. Expected range of E_{pk}

Photospheric emission from dissipative jets is affected by beaming and photon production as shown in Figure 1. Beaming increases the apparent luminosity, and photon production reduces the observed E_{pk} . Adiabatic cooling needs not to be considered, as the dissipative jets maintain $L_\gamma \sim L$.

Reasonable beaming factors $L/L_0 \sim 10^2$ (which are suggested by the burst energetics and the afterglow data analysis) together with the expected photon production in a dissipative jet naturally explain the location of observed GRBs on the $L_\gamma-E_{\text{pk}}$ diagram (approximately shown by the yellow strip in Figure 1). The observed bursts are also consistent with $R_P \sim 10^{10}$ cm (Equation 47). The estimated Lorentz factor at the Planck

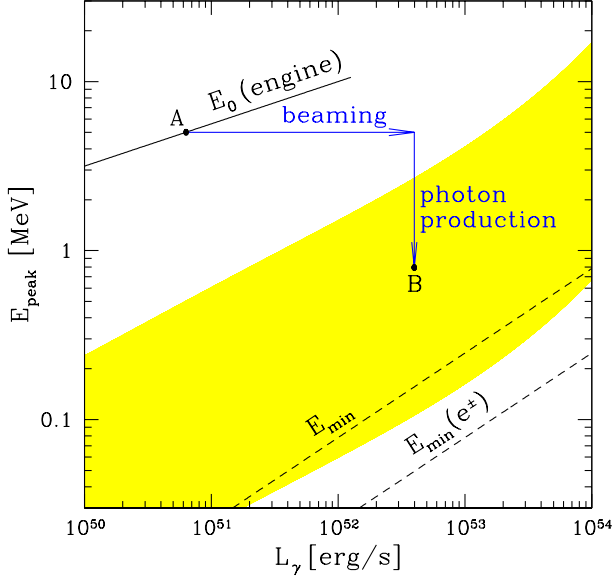


FIG. 1.— L_γ - E_{pk} diagram. Point A is an example of the initial condition near the central engine; the jet starts with E_{pk} close to E_0 (Equation 3). As the jet expands, its apparent luminosity L_γ is increased by beaming and E_{pk} is reduced by photon production. Point B shows the resulting photospheric emission. The approximate region populated by observed GRBs is shown in yellow. The observed E_{pk} should not violate the lower bound E_{min} that is set by the effective blackbody temperature of the photospheric radiation (Equation 49). Dashed line shows E_{min} given by Equation (50) with $q = 1$. Dashed line marked $E_{\text{min}}(e^\pm)$ allows for the presence of e^\pm pairs with multiplicity $f_\pm = 10$.

radius, $\Gamma_P \sim 30(E_{\text{pk}}/\text{MeV})$ (Equation 42), is consistent with a slow jet acceleration in the zone $r_0 < r < R_P$, as expected in the presence of a strong collimation.

Accurate theoretical predictions for the burst locations on the diagram are difficult; however, one can estimate the lower and upper bounds on E_{pk} . The lower bound is obtained from the fact that the photospheric emission cannot be colder than the effective blackbody temperature, which is defined by Equation (4).

$$E_{\text{min}} \approx 4\Gamma k T_{\text{eff}} = 2 \left(\frac{45}{\pi^3} \right)^{1/4} \left(\frac{\Gamma}{R_\star} \right)^{1/2} (L_\gamma c^2 \hbar^3)^{1/4}. \quad (48)$$

Substitution of Equation (39) for R_\star gives

$$E_{\text{min}} \approx 4 \left(\frac{45}{\pi} \right)^{1/4} \frac{\epsilon^{1/4}}{f_\pm^{1/2}} \eta^{1/2} \Gamma^{3/2} \left(\frac{m_p^2 c^8 \hbar^3}{L \sigma_T} \right)^{1/4} \\ \approx 40 \frac{\eta_2^{1/2} \Gamma_2^{3/2} \epsilon^{1/4}}{L_{52}^{1/4} f_\pm^{1/2}} \text{ keV}, \quad (49)$$

where $\epsilon = L_\gamma/L \sim 1$ is the radiative efficiency, and $f_\pm = 1 + n_\pm/n$ describes the increase of R_\star due to possible e^\pm creation.

Equation (49) may be simplified if there is a relation between L and Γ (or η). The existence of such a relation in GRBs is uncertain. Model-dependent analysis of afterglow light curves by Ghirlanda et al. (2012) and Lü et al. (2012) suggests an approximate correlation $\Gamma \propto L^m$ with m between 1/4 and 1/2. This (debatable) correlation may motivate one to consider a relation of the form

$\Gamma_2^2 = q L_{\gamma,52}^{3/4}$, where $q \sim 1$ is a factor that may weakly depend on L_γ . With such parametrization, E_{min} becomes proportional to $L^{1/2}$,

$$E_{\text{min}} \approx 40 q L_{52}^{1/2} f_\pm^{-1/2} \text{ keV}, \quad (50)$$

where $\epsilon \sim 1$ and $\Gamma \approx \eta$ have been assumed at the photosphere.

The upper bound on E_{pk} for thermally dominated jets is set by the initial conditions near the central engine. The spectrum of radiation carried by the jet peaks at photon energy slightly above \bar{E} , e.g. $E_{\text{pk}} = (4/3)\bar{E}$ for a Wien spectrum. The highest \bar{E} is set by the jet energy per photon near the central engine,

$$E_0 \approx 2.7kT_0, \quad aT_0^4 = U_0, \quad (51)$$

where U_0 is the energy density at the base of the jet.⁶ The energy density is related to the jet power L_0 by

$$L_0 = \Omega_0 r_0^2 U_0 c \beta_0, \quad (52)$$

where Ω_0 is the opening solid angle of the flow near the central engine, and $\beta_0 = v_0/c \sim 1$ is the flow velocity. This gives

$$E_0 \approx 10 \left(\beta_0 \frac{\Omega_0}{4\pi} \right)^{-1/4} L_{0,52}^{1/4} r_{0,6}^{-1/2} \text{ MeV}. \quad (53)$$

If the central engine is an accreting black hole, r_0 is comparable to a few Schwarzschild radii $r_g = 2GM/c^2$, and the maximum possible power L_0 is comparable to the accretion power,

$$L_{\text{acc}} \sim \frac{GM\dot{M}_{\text{acc}}}{r_0} \approx 3 \times 10^{53} \dot{m} \left(\frac{r_0}{3r_g} \right)^{-1} \text{ erg s}^{-1}, \quad (54)$$

where \dot{m} is the accretion rate \dot{M}_{acc} in units of $M_\odot \text{ s}^{-1}$. Ratio L_0/L_{acc} describes the efficiency of energy deposition at the base of the jet; it is expected to be small. The only robust heating mechanism is neutrino-antineutrino annihilation, which gives (Zalamea & Beloborodov 2011)

$$L_0 \approx 10^{52} \dot{m}^{9/4} x_{\text{ms}}^{-4.8} \left(\frac{M}{3M_\odot} \right)^{-3/2} \text{ erg s}^{-1}. \quad (55)$$

Here x_{ms} is the radius of the marginally stable Keplerian orbit in units of r_g ; it is determined by the spin parameter of the black hole a and varies between $x_{\text{ms}} = 3$ for $a = 0$ and $x_{\text{ms}} = 1/2$ for $a = 1$. Optimistic assumptions regarding the black hole spin give $x_{\text{ms}} \approx 1$ (which corresponds to $a = 0.95$). In this case, heating peaks in a region of radius $r_0 \sim 3r_g \approx 10^6 (M/3M_\odot)$ cm. Note that the maximum $L_0 \sim 10^{52} \text{ erg s}^{-1}$ corresponds to a minimum $r_0 \sim 10^6$ cm.

The thermal jet power L_0 is sensitive to the accretion rate and the black hole spin. It can vary by several orders of magnitude, which implies large variations in observed

⁶ A more accurate expression for U_0 includes the contribution from e^\pm pairs. The corresponding correction to T_0 (the reduction by a factor of $[4/11]^{1/4}$) is compensated by additional photon energy that appears in the expanding jet when the e^\pm pairs cool down and annihilate. Therefore, one can use the simplified Equation (51) for the estimate of the maximum \bar{E} at radii $r \gg r_0$.

luminosity (even when the beaming angle θ_b remains unchanged). The maximum $L_0 \sim 10^{52}$ erg s $^{-1}$ corresponds to the maximum achievable E_{pk} of 10-15 MeV.

4. MAGNETICALLY DOMINATED JETS

It is possible that the energy output of the central engine is dominated by the Poynting flux, i.e. carried mainly by the magnetic field. Then the total energy per proton (cf. Equation 5) is given by

$$\eta = \eta_B + \eta_{\text{th}} = \text{const.} \quad (56)$$

Near the central engine the contribution of the thermal power is small, $\epsilon = \eta_{\text{th}}/\eta \ll 1$; it can increase at larger radii at the expense of the magnetic part η_B/η . The magnetic field is the main reservoir of energy and a large fraction of it must dissipate if the model aims to describe a bright, radiatively efficient burst.

Energy dissipated at radii $r < R_P$ must be thermalized into Planck radiation with luminosity $L_\gamma(R_P) = \eta_P \dot{M} c^2$ (where $\eta_P = \eta_{\text{th}}[R_P]$) and with the average photon energy

$$\bar{E}_P = \eta_P m_p c^2 \left(\frac{n}{n_\gamma} \right)_{R_P}. \quad (57)$$

At $r > R_P$ the photon-to-baryon ratio freezes out (as long as the main photon producer is the thermal plasma, i.e. nonthermal processes are less efficient). As dissipation continues in the Wien zone $r > R_P$, \bar{E} grows proportionally to η_{th} . The observed E_{pk} is associated with \bar{E}_W at $r \sim R_W$,

$$\bar{E}_W \approx \frac{\eta_W}{\eta_P} \bar{E}_P = \frac{\eta_W m_p c^2}{(n_\gamma/n)_{R_P}}, \quad (58)$$

where $\eta_W = \eta_{\text{th}}(R_W)$. Equation (58) shows that E_{pk} could be very high if the Planck zone is cold (which gives a small n_γ/n) and the Poynting flux dissipation is strong in the Wien zone (which gives a high η_W). Such a jet would experience ‘‘photon starvation’’ — the dissipated energy would be carried by a small number of photons with a high energy per photon, hence a high E_{pk} . This suggests that E_{pk} in magnetically dominated jets may exceed the maximum E_{pk} of thermally dominated jets.

More specific estimates can be made as follows. Magnetically dominated jets are expected to start with a modest Lorentz factor at the Alfvén radius and then gradually accelerate. In a simple self-similar model, the dissipated Poynting flux is distributed in comparable amounts between the thermal luminosity L_γ (dominated by radiation) and the proton kinetic energy flux, L_{kin} . This means that $\eta_{\text{th}} \approx \Gamma$ and the thermal energy density in the fluid frame is approximately equal to the proton rest-mass density,

$$U_\gamma \approx 3kT n_\gamma \approx m_p c^2 n, \quad (59)$$

which gives a simple relation between the jet temperature and the photon-to-baryon ratio,

$$\frac{n_\gamma}{n} \approx \frac{m_p}{3m_e \Theta}. \quad (60)$$

The freeze-out of n_γ/n implies approximately constant temperature $\Theta = kT/mc^2$ at $r > R_P$, i.e. the jet temperature in the Wien zone remains approximately equal

to T_P . This fact may be understood in a slightly different way: conservation of the photon flux in the Wien zone implies $L_\gamma \propto \bar{E} \approx 4\Gamma kT$; then the scaling $L_\gamma \approx L_{\text{kin}} \propto \Gamma$ requires $T = \text{const} = T_P$.

From Equation (20) we have

$$\Theta_P \approx 0.01 \left(\frac{R_P}{10^{10} \text{ cm}} \right)^{-1/6} \left(\frac{\eta_P}{30} \right)^{1/6}. \quad (61)$$

Substitution of $\Theta = \Theta_P$ into Equation (60) gives the photon-to-baryon ratio for magnetically dominated jets,

$$\frac{n_\gamma}{n} \approx 6 \times 10^4. \quad (62)$$

The observed E_{pk} is close to $\bar{E}_W = 4\Gamma_W kT_W$, where $\Gamma_W = \Gamma(R_W)$ and $T_W = T(R_W) \approx T_P$ is unchanged from the temperature at Planck radius T_P . This gives

$$E_{\text{pk}} \approx 3 \left(\frac{\Gamma_W}{100} \right) \text{ MeV}. \quad (63)$$

In a radiatively efficient GRB dominated by photospheric emission, magnetic dissipation is expected to be nearly complete at subphotospheric radii (but see Section 5.2). Then Γ_W may be comparable to the asymptotic value, $\Gamma_W \lesssim \eta$.

A monotonic dependence of E_{pk} on Γ or η is generally expected for magnetically dominated jets. Giannios (2012) estimated E_{pk} assuming blackbody radiation $T = T_{\text{eff}}$ in the Wien zone $y \gg 1$. He found $E_{\text{pk}} \propto \Gamma^{4/3} \eta^{1/3}$, which gives $\eta^{5/3}$ if $\Gamma \sim \eta$. Comparison of Equation (8) in Giannios (2012) with our Equation (63) shows how the photon deficit in the Wien zone affects the observed spectral peak. E_{pk} is significantly higher, in particular for moderate $\eta \sim 100$, and the scaling with η is linear if $\Gamma_W \sim \eta$.

E_{pk} could be increased above the estimate (63) if magnetic dissipation is delayed so that heating is strongly suppressed at $r < R_P$. Then $U_\gamma \ll n m_p c^2$ at the Planck radius, and the jet can be in the regime of a strong photon starvation. This regime would, however, require a very cold central engine, to avoid thermal photons transported by the jet from the center.

In fact, the model described by Equations (59)-(63) already implies a relatively cold central object. It assumes that the density of heat advected from the center to R_P is smaller than the heat generated by magnetic dissipation, and smaller than $n m_p c^2$. The model assumes that the initial thermal energy per baryon $\eta_{\text{th},0}$ becomes dynamically unimportant (unable to accelerate the jet) before the temperature drops to T_P . Only in this case the jet dynamics and photon number at R_P are controlled by magnetic dissipation rather than by heat advected from the central engine. This condition requires an initial temperature

$$T_0 \lesssim \eta_{\text{th},0} T_P \approx 5 \eta_{\text{th},0} \text{ keV}. \quad (64)$$

Magnetically dominated models assume $\eta_{\text{th},0} \ll \eta$, which leads to a strong upper bound on T_0 . It would be inconsistent, for instance, with the collapsar model that invokes a hot accretion disk with strong neutrino emission. A relatively cold central engine is expected in the proto-magnetar model (e.g. Metzger et al. 2011).

5. DISCUSSION

5.1. Regulation of E_{pk}

Three characteristic radii are important for the formation of a photospheric GRB spectrum:

(1) Planck radius R_{P} below which radiation is forced to have a Planck spectrum. GRB jets have a well-defined temperature $\Theta_{\text{P}} \approx 0.01$ and Thomson optical depth $\tau_{\text{P}} \approx 10^5$ at the Planck radius. The typical value of R_{P} is 10^{10} cm (Equation 47).

(2) Wien radius R_{W} below which $y \gg 1$ and radiation maintains a Wien (or Bose-Einstein) spectrum. Compton scattering enforces thermal coupling between the electrons and photons at $r < R_{\text{W}}$; however, the radiation density can be far below the blackbody density aT^4 . The Wien zone $R_{\text{P}} < r < R_{\text{W}}$ occupies an extended range of optical depths, $\tau_{\text{P}} > \tau > \tau_{\text{W}}$, where $\tau_{\text{W}} \sim 10^2$. The existing transfer simulations indicate that the observed E_{pk} is inherited from the Wien zone.

(3) Photospheric radius R_{\star} where optical depth $\tau = 1$. Radiation is released around R_{\star} . Thermal decoupling of plasma and radiation, $T_e > T_{\gamma}$, occurs in the zone $R_{\text{W}} < r < R_{\star}$, and Comptonization changes the released spectrum from Wien to Band shape.

It is instructive to consider the role of entropy for the regulation of E_{pk} . Entropy of GRB jets is strongly dominated by radiation. Entropy of Planck radiation is proportional to photon number. In a non-dissipative jet (whose entropy is conserved) radiation keeps a Planck spectrum even outside R_{P} , as this is consistent with constant photon number — the production of additional photons is not needed to maintain the thermal spectrum.

In dissipative jets, maintaining a Planck spectrum requires a growing photon number, which is possible as long as there are sufficiently fast processes producing photons. Such processes are guaranteed at $r < R_{\text{P}}$. Outside R_{P} , the thermal plasma becomes unable to supply new photons; then the photon number freezes out and does not keep up anymore with the Planck value. This leads to the photon deficit $n_{\gamma} < n_{\text{P}}$ and the Wien spectrum between R_{P} and R_{W} . Photon deficit could be avoided if a significant fraction of the dissipated energy is injected in the form of nonthermal particles; then additional photons could be generated by synchrotron emission (Section 2.5; Urum et al. 2012). However, the efficiency of nonthermal particle injection in the (very opaque) Wien zone is uncertain; in addition, the synchrotron photon supply is reduced by Bose condensation (Urum et al. 2012).

In general, photospheric emission with efficiency $\epsilon = L_{\gamma}/L$ and photon-to-baryon ratio n_{γ}/n satisfies the following relation,

$$\frac{E_{\text{pk}}}{E_0} \approx \frac{\epsilon}{\epsilon_0} \frac{(n_{\gamma}/n)_0}{(n_{\gamma}/n)}, \quad (65)$$

where index “0” refers to the radius r_0 of the central engine; ϵ_0 is the initial thermal fraction of the jet and E_0 is given in Equation (3). Note that the photon number never decreases below its central value (dissipation can only increase it), i.e. $Q = (n_{\gamma}/n)(n_{\gamma}/n)_0^{-1} \geq 1$. Equation (65) is applicable to both thermally dominated ($\epsilon_0 \approx 1$) and magnetically dominated ($\epsilon_0 \ll 1$) jets; it is valid regardless of dissipation or collimation mechanisms.

Non-dissipative flows have $Q = 1$ and preserve a Planck spectrum everywhere in the opaque zone $r \ll R_{\star}$.⁷ The resulting $E_{\text{pk}} = (\epsilon/\epsilon_0)E_0$ is determined by the adiabatic cooling factor $\epsilon/\epsilon_0 < 1$, which is related to the radiative efficiency of photospheric emission ϵ .

Dissipation affects E_{pk} in two ways. Since heat is quickly passed to radiation, strong subphotospheric dissipation gives a high radiative efficiency $\epsilon \sim 1$, offsetting the adiabatic cooling effect (and in magnetic jets that start with a small thermal fraction $\epsilon_0 \ll 1$, $\epsilon > \epsilon_0$ is possible). On the other hand, dissipation tends to generate photons, in particular in the Planck zone, where the photon number grows proportionally to the generated entropy. The observed E_{pk} is sensitive to the photon production factor Q . Typical observed GRBs are consistent with $Q \sim 10$ (Figure 1), suggesting significant dissipation in the Planck zone. One can also see that bursts with record-high $E_{\text{pk}} \sim 10 - 20$ MeV (Axelsson et al. 2012) must have $Q \sim 1$ (the minimum possible value) or be magnetically dominated near the central engine, $\epsilon_0 \ll 1$.

The lower bound on E_{pk} is derived if one assumes unlimited photon production that maintains detailed equilibrium up to the photosphere. This would give a blackbody photospheric emission with $E_{\text{pk}} \approx E_{\text{min}}$ given by Equation (49). The condition $E_{\text{pk}} > E_{\text{min}}$ gives a robust upper bound on the jet Lorentz factor,

$$\Gamma < 270 \left(\frac{E_{\text{pk}}}{300 \text{ keV}} \right)^{1/2} L_{\gamma,52}^{1/8} f_{\pm}^{1/4} \epsilon^{-1/4}, \quad (66)$$

where $f_{\pm} = 1 + n_{\pm}/n$ is the pair loading factor.

In the thermally dominated limit, $\eta_{\text{th}} \gg \eta_B$, the maximum value for E_{pk} is set by the initial temperature near the central engine (Equation 51). A plausible scenario invokes comparable contributions of the initial thermal energy and magnetic field to the jet power, $\eta_{\text{th}} \sim \eta_B$. Then the maximum $E_{\text{pk}} \sim 10$ MeV expected for the pure thermal jet can be increased by a factor ~ 2 by dissipation of additional magnetic energy that has been transported by the Poynting flux to $r > R_{\text{P}}$. This picture is consistent with the observed distribution of E_{pk} , which cuts off at about 20 MeV.

In the magnetically dominated limit, $\eta_B \gg \eta_{\text{th}}$, the initial temperature plays no role. In this case, the thermal output of the central engine is negligible and heat/photons are gradually generated in the expanding jet as a result of magnetic dissipation. The simple self-similar model gives a unique $n_{\gamma}/n \sim 6 \times 10^4$ at the Planck radius, and the observed E_{pk} is proportional to the Lorentz factor of the jet (Equation 63).

5.2. Magnetic dissipation

The rate of magnetic dissipation is hard to calculate from first principles; e.g., the reconnection rate depends on the field structure in the jet. Theory is easily reconciled with observations if most of dissipation occurs at subphotospheric radii, $R_{\text{diss}} < R_{\star}$. The MeV peak is observed to carry most of the GRB energy, and we argued in Section 1 that it emerges from the photosphere, which implies that most of electron heating occurs at $r < R_{\star}$.

⁷ Transfer effects near the photosphere R_{\star} modify the observed spectrum into a multi-Doppler-shifted blackbody (Beloborodov 2010; Pe’er & Ryde 2011).

The photospheric radius steeply decreases with Γ , $R_\star \propto \Gamma^{-3}$, while R_{diss} increases with Γ , e.g. in the magnetic dissipation model of Drenkhahn & Spruit (2002). Then the condition $R_{\text{diss}} < R_\star$ typically means $R_{\text{diss}} \ll R_\star$ (as $R_{\text{diss}} \sim R_\star$ would require fine-tuning of Γ). This feature of magnetic dissipation is avoided only in models with reconnection rate suppressed at $\tau \gg 1$ and quickly increasing at $\tau \sim 1$ (Mckinney & Uzdensky 2012).

If dissipation peaks at $r < R_W$, it must influence E_{pk} . In this scenario, the dissipation of the energetically dominant Poynting flux is hidden at high optical depths, and it does not dominate the heating at $r \lesssim R_\star$ where the Wien spectrum is Comptonized into a Band shape.

The remaining source of energy in the Comptonization zone is internal bulk motions (which may be initiated by magnetic dissipation at smaller radii). In particular, collisional dissipation, which provides significant electron heating, is expected to peak at moderately subphotospheric radii $r \lesssim R_\star$. It begins at $R_n \sim (\sigma_n/\sigma_T)R_\star$, where $\sigma_n \approx \sigma_T/20$ is the nuclear cross section, and converts a large fraction of the jet energy to electron heat and nonthermal e^\pm pairs.

Models that invoke strong magnetic dissipation extending through the photosphere may be consistent with observations if the released energy is given to protons, and electrons receive energy from protons via Coulomb collisions. Coulomb coupling is efficient only below the photosphere; therefore, electrons receive and radiate the dissipated energy at subphotospheric radii $r < R_\star$. (At radii $r > R_\star$ most of the proton heat is not radiated — it is lost to adiabatic cooling and converted to the bulk kinetic energy of the jet.) This scenario is a “magnetically powered” variation of the collisional mechanism. The heating of protons results in bright emission due to e - p Coulomb energy exchange. In addition, it may lead to inelastic nuclear p - p collisions; this process will inject e^\pm pairs with Lorentz factors $\gamma \sim m_\pi/m_e \sim 300$ and generate an extended high-energy tail of the GRB spectrum. This model is similar to that of Beloborodov (2010), which examined n - p collisions. The only difference is that here the source of heat is the magnetic field instead of the relative streaming of the neutron and proton components of the jet.

5.3. Variations in E_{pk}

Various reported correlations between E_{pk} , L_γ , and Γ may be compared with theoretical predictions for photospheric emission (e.g. Giannios 2012; Fan et al. 2012). We argued in this paper that one should not make blackbody assumptions in this analysis; instead, one should examine the entire expansion history of the jet. Besides the energy output of the central engine, L_0 , and its thermal fraction ϵ_0 , the observed emission is controlled by two factors: beaming L/L_0 and the photon production factor Q (Figure 1). Photon production depends on dissipation in the Planck zone due to collimation shocks, or possibly due to magnetic reconnection.

A positive correlation between E_{pk} and the burst luminosity is expected for dissipative jets; e.g. thermally dominated jets with fixed $r_0 = \text{const}$ and beaming angle $\theta_b = \text{const}$ would have E_{pk} scaling as $L_\gamma^{1/4}$. The E_{pk} - L_γ correlation steepens in the presence of magnetic dissipation if brighter bursts have higher Γ . The relation between L and E_{pk} can also be affected by a correlation between the jet opening angle θ_b and the photon production factor Q .

Low E_{pk} is naturally associated with a large Q . It is also associated with a low true luminosity L_0 (and the correspondingly low central temperature T_0). A strong collimation can boost the apparent luminosity L from a low L_0 , however it cannot increase E_{pk} (Section 3).

The dependence of E_{pk} on luminosity L and photon number helps understand the pattern of E_{pk} variations in individual pulses of GRB light curves. Although a tracking behavior $E_{\text{pk}}(L)$ is expected, the presence of the second parameter can lead to significant deviations. In particular, the observed high E_{pk} at the beginning of a pulse (before its luminosity reaches maximum) may be explained as emission with a low photon-to-baryon ratio. As the pulse progresses, n_γ/n grows until the normal tracking behavior is established. In addition, the observed L depends on the beaming factor, which may vary during the burst; this may also contribute to the deviations from the tracking behavior $E_{\text{pk}}(L)$.

I thank Amir Levinson and Indrek Vurm for useful comments on the manuscript. This work was supported by NSF grant AST-1008334.

APPENDIX

A. PHOTON PRODUCTION RATES

The rate of photon production by the double Compton effect has been extensively discussed in the literature (e.g. Thorne 1981; Lightman 1981; Pozdnyakov et al. 1983; Svensson 1984; Chluba et al. 2007). Scattering of monoenergetic photons of energy $h\nu_0$ and density n_γ on cold electrons of density n produces secondary photons $h\nu$ with the following differential rate,

$$\frac{d\dot{n}_{\text{DC}}}{d\ln\nu} = \frac{4\alpha}{3\pi} n n_\gamma \sigma_T c \left(\frac{h\nu_0}{m_e c^2} \right)^2, \quad (\text{A1})$$

where $\alpha = e^2/\hbar c = 1/137$ is the fine structure constant. Equation (A1) is valid when the secondary photon has energy $h\nu \ll h\nu_0$. Extension to $\nu \sim \nu_0$ was discussed by Gould (1984); it gives only a small correction to the total photon production rate \dot{n}_{DC} , as \dot{n}_{DC} has a flat distribution over $\ln\nu$ and most photons are emitted with $\nu \ll \nu_0$.

For primary photons $h\nu_0$ with a given spectrum, rate (A1) should be averaged over the spectrum. For a Bose-Einstein radiation with temperature T , this gives

$$\frac{d\dot{n}_{\text{DC}}}{d\ln x} = \frac{4\alpha}{3\pi} n n_\gamma \sigma_T c x_0^2 \Theta^2, \quad x_0 = \frac{h\nu_0}{kT}, \quad x = \frac{h\nu}{kT}, \quad \Theta = \frac{kT}{m_e c^2}, \quad (\text{A2})$$

where $\overline{x_0^2} = 12\zeta(5)/\zeta(3) \approx 10.35$ for a Planck spectrum and $\overline{x_0^2} = 12$ for a Wien spectrum; photons with $x_0 \gtrsim 1$ make the dominant contribution.

The net rate \dot{n}_{DC} is obtained by integrating Equation (A2) over x from a minimum value x_{min} to $x \sim 1$. Here x_{min} is a minimum energy of produced photons that avoid absorption and get a chance to be Comptonized to the Wien peak (Thorne 1981; Lightman 1981). It is determined by equating the absorption rate $t_{\text{abs}}^{-1} = a_{\text{DC}} c$ (where a_{DC} is the absorption coefficient due to inverse double Compton effect) and the Comptonization rate t_{IC}^{-1} (where t_{IC} is the time it takes to Comptonize the photon energy by a factor of 2). Absorption coefficient a_{DC} is found from Kirchhoff's law for Rayleigh-Jeans radiation $a_{\text{DC}} 8\pi\nu^2 kT/c^2 = h\nu d\dot{n}_{\text{DC}}/d\nu$. Comptonization rate at non-relativistic temperatures is $t_{\text{IC}}^{-1} \approx 4\Theta n\sigma_{\text{T}}c$. This gives,

$$x_{\text{min}} = \left(\frac{\pi}{3} \alpha \lambda^3 n_{\gamma} \overline{x_0^2} \Theta^{-2}\right)^{1/2} = \left(\frac{8}{\pi} \alpha \zeta(5) \Theta\right)^{1/2} \approx 0.14\Theta^{1/2}, \quad (\text{A3})$$

where $\lambda = \hbar/m_e c$ is Compton wavelength. We have used the relation $\lambda^3 n_{\gamma} \overline{x_0^2} = (24/\pi^2)\zeta(5) \Theta^3$ for blackbody radiation, where $\zeta(5) \approx 1.037$. Integration of Equation (A2) gives

$$\dot{n}_{\text{DC}} = \chi n n_{\gamma} \sigma_{\text{T}} c \Theta^2, \quad \chi = \frac{4\alpha}{3\pi} \overline{x_0^2} \ln x_{\text{min}}^{-1}. \quad (\text{A4})$$

This equation assumes that the scattering electrons are cold in the sense that $\Theta \ll 1$. In the case of a hot plasma it should be multiplied by a correction factor that has been obtained by Svensson (1984) (see also Chluba et al. 2007). The correction factor is given by

$$g_{\text{DC}} = (1 + 13.91\Theta + 11.05\Theta^2 + 19.9\Theta^3)^{-1}. \quad (\text{A5})$$

At the boundary of the Planck zone we find $\Theta_{\text{P}} \approx 10^{-2}$ (Section 2.2); then $\chi \approx 0.1$.

Photon production by bremsstrahlung is given by (e.g. Illarionov & Sunyaev 1975; Thorne 1981; Pozdnyakov et al. 1983),

$$\frac{d\dot{n}_{\text{B}}}{d\ln x} = \left(\frac{2}{\pi}\right)^{3/2} \alpha n^2 \sigma_{\text{T}} c \Theta^{-1/2} \ln \frac{2.2}{x}. \quad (\text{A6})$$

Relativistic corrections (e.g. Svensson 1984) are small for temperatures of interest here. Comparison with Equation (A2) shows that at relevant temperature $\Theta_{\text{P}} \gtrsim 0.01$ and photon-to-baryon ratio $n_{\gamma}/n \sim 10^5$, the bremsstrahlung emissivity is smaller or comparable to the double Compton emissivity. Integration of Equation (A6) over $\ln x$ from $\ln x_{\text{min}}$ to $\ln x \sim 0$ gives

$$\dot{n}_{\text{B}} = \xi n^2 \sigma_{\text{T}} c \Theta^{-1/2}, \quad \xi \approx \left(\frac{2}{\pi}\right)^{3/2} \alpha (\ln x_{\text{min}}^{-1})^2. \quad (\text{A7})$$

Near the boundary of the Planck zone $\xi \approx 0.06$.

REFERENCES

- Axelsson, M., et al. 2012, *ApJ*, 757, L31
Band, D. L., et al. 2009, *ApJ*, 701, 1673
Baring, M. G., & Braby, M. L. 2004, *ApJ*, 613, 460
Beloborodov A. M., 2003, *ApJ*, 588, 931
Beloborodov, A. M. 2010, *MNRAS*, 407, 1033
Beloborodov, A. M. 2011, *ApJ*, 737, 68
Burgess, J. M., et al. 2011, *ApJ*, 741, 24
Chluba, J., Sazonov, S. Y., & Sunyaev, R. A. 2007, *A&A*, 468, 785
Daigne, F., Bosnjak, Z., & Dubus, G. 2011, *A&A*, 526, A110
Drenkhahn, G., & Spruit, H. C. 2002, *A&A*, 391, 1141
Eichler, D., & Levinson, A. 2000, *ApJ*, 529, 146
Fan, Y.-Z., et al. 2012, *ApJ*, 755, L6
Giannios, D. 2008, *A&A*, 480, 305
Giannios, D. 2012, *MNRAS*, 422, 3092
Ghirlanda, G., Ghisellini, G., & Nava, L. 2011, *MNRAS*, 418, L109
Ghirlanda, G., Nava, L., Ghisellini, G., et al. 2012, *MNRAS*, 420, 483
Ghisellini, G. 2006, in *VI Microquasar Workshop: Microquasars and Beyond*, 27 (arXiv:astro-ph/0611077)
Goldstein, A., et al. 2012, *ApJS*, 199, 19
Goodman, J. 1986, *ApJ*, 308, L47
Gould, R. J. 1984, *ApJ*, 285, 275
Illarionov, A. F., & Sunyaev, R. A. 1975, *Sov. Astr.*, 18, 413
Kaneko, Y., et al. 2006, *ApJS*, 166, 298
Lü, J., et al. 2012, *ApJ*, 751, 49
Lazzati, D., Morsony, B. J., & Begelman, M. C. 2009, *ApJ*, 700, L47
Levinson, A. 2012, *ApJ*, 756, 174
Lightman, A. P. 1981, *ApJ*, 244, 392
McKinney, J. C., & Uzdensky, D. A. 2012, *MNRAS*, 419, 573
Metzger, B. D., Thompson, T. A., & Quataert, E. 2008, *ApJ*, 676, 1130
Paczynski, B. 1986, *ApJ*, 308, L43
Paczynski, B. 1990, *ApJ*, 363, 218
Pe'er, A., Mészáros, P., & Rees, M. J. 2006, *ApJ*, 642, 995
Pe'er, A., & Ryde, F. 2011, *ApJ*, 732, 49
Pozdnyakov, L. A., Sobol, I. M., & Sunyaev, R. A. 1983, *Astrophys. Space Phys. Rev.*, 2, 189
Rees, M. J., & Mészáros, P. 1994, *ApJ*, 430, L93
Rees, M. J., & Mészáros, P. 2005, *ApJ*, 628, 847
Ryde, F., et al. 2011, *MNRAS*, 415, 3693
Shemi, A., & Piran, T. 1990, *ApJ*, 365, L55
Sironi, L., & Spitkovsky, A. 2011, *ApJ*, 726, 75
Svensson, R., 1984, *MNRAS*, 209, 175
Thompson, C., Mészáros, P., & Rees, M. J. 2007, *ApJ*, 666, 1012
Thorne, K. S. 1981, *MNRAS*, 194, 439
Vurm, I., Beloborodov, A. M., & Poutanen, J. 2011, *ApJ*, 738, 77
Vurm, I., Lyubarsky, Y., & Piran, T. 2012, arXiv:1209.0763
Yonetoku, D., et al. 2004, *ApJ*, 609, 935
Zalamea, I., & Beloborodov, A. M. 2011, *MNRAS*, 410, 2302
Wei, D. M., & Gao, W. H. 2003, *MNRAS*, 345, 743